TU Delft

Delft University of Technology

Document Version
Final published version

Licence
Dutch Copyright Act (Article 25fa)

Citation (APA)
Li, C., Zheng, K., Vergara Barrios, P. P., Zhang, N., & Guo, H. (2026). A Projection Method for Aggregating Large-Scale DERs with Heterogeneity. *IEEE Transactions on Smart Grid*, *17*(3), 2092-2104. https://doi.org/10.1109/TSG.2025.3650457

Important note
To cite this publication, please use the final published version (if applicable).
Please check the document version above.

Copyright
In case the licence states “Dutch Copyright Act (Article 25fa)”, this publication was made available Green Open Access via the TU Delft Institutional Repository pursuant to Dutch Copyright Act (Article 25fa, the Taverne amendment). This provision does not affect copyright ownership.
Unless copyright is transferred by contract or statute, it remains with the copyright holder.

Sharing and reuse
Other than for strictly personal use, it is not permitted to download, forward or distribute the text or part of it, without the consent of the author(s) and/or copyright holder(s), unless the work is under an open content license such as Creative Commons.

Takedown policy
Please contact us and provide details if you believe this document breaches copyrights.
We will remove access to the work immediately and investigate your claim.

This work is downloaded from Delft University of Technology.

A Projection Method for Aggregating Large-Scale DERs With Heterogeneity

Chuyi Li, *Graduate Student Member, IEEE*, Kedi Zheng, *Member, IEEE*, Pedro P. Vergara, *Senior Member, IEEE*, Ning Zhang, *Senior Member, IEEE*, and Hongye Guo, *Member, IEEE*

***Abstract*—The power consumption flexibility of distributed energy resources (DERs) must be aggregated to enable effective interaction with power systems. However, model heterogeneity, geographical dispersion, and the large number pose significant challenges to aggregation. This paper first models DER flexibility by explicitly incorporating heterogeneity in both state variables and available time periods, represented through polytopes of heterogeneous dimensions. The aggregation of DERs is then formulated as a standard projection maximal inner approximation (MIA) problem. To efficiently and accurately solve this problem, a novel linear programming (LP)-based algorithm is developed. Furthermore, a hierarchical framework is introduced to enable large-scale aggregation, within which a Minkowski-closed family is proven, allowing accurate and efficient secondary aggregation through vector addition. In addition, generalized operating envelopes (OEs) are proposed for distribution system operators (DSOs) to establish and communicate network constraints, enabling integration into the aggregation process without disclosing sensitive network information. Numerical experiments validate the proposed formulations and demonstrate superior accuracy and scalability of the proposed method while maintaining high computational efficiency.**

***Index Terms*—Distributed energy resources, aggregation, polytope, projection, Minkowski sum, operating envelope.**

I. Introduction

THE rise in the penetration rate of renewable energy poses significant challenges to the operation of the system, highlighting the shortage of flexibility. Meanwhile, the rapid development of grid intelligence has led to a growing presence of flexible distributed energy resources (DERs), such as photovoltaics (PVs), heating-ventilating-and-air-conditioning systems (HVACs), and electric vehicles (EVs). In a traditional system operation, electricity demand is considered rigid and must be balanced in real-time by generators. However, many demands have an elastic range. In fact, numerous flexible loads are dispersed within the distribution network, capable of collaborating with distributed generation resources to provide energy or regulation services [1]. Releasing this potential is difficult due to insufficient capacity or a lack of incentives for individuals. A widely adopted solution is to aggregate DERs as one entity to provide flexibility for the grid [2].

With virtual power plant (VPP) technology, aggregators can manage massive DERs connected across multiple nodes in a distribution network. By collecting the operational data and parameters of these DERs, an aggregator can represent them as a single entity for interaction with the grid. However, DERs in distribution networks are typically heterogeneous in flexibility models, dispersed throughout the system, and numerous. The diverse physical and operational characteristics of these resources make direct aggregation challenging. The distribution system must manage power injections from DERs to ensure operational safety. Additionally, large-scale aggregation introduces significant computational complexity. Efficient aggregation of DERs thus remains a critical problem requiring further investigation.

A. Related Works

To model the power flexibility of DERs, a polytope-based approach was first proposed in [3] and has since been widely adopted [4], [5]. In this approach, each DER is represented as a polytope defined by a system of linear constraints, which capture the state equations as well as the upper and lower bounds on interface power consumption and internal state variables. The aggregation process aims to construct a single representative model that captures the collective flexibility of a group of DERs, abstracting away internal variables that are irrelevant to external coordination. Mathematically, this involves computing the geometric sum of the individual polytopes, known as the Minkowski sum. However, calculating the Minkowski sum is an NP-hard problem [6]. Researchers have focused on developing approximation methods. Barot and Taylor [3] proposed a linear programming (LP)-based outer approximation algorithm that is computationally efficient. Nevertheless, outer approximations can lead to disaggregation infeasibility, which may result in significant penalties from the market. For inner approximations, several geometrical forms have been explored, including boxes [7], ellipses [8], and zonotopes [4]. Zhao et al. [9] introduced a scaling and translation method for polytope maximal inner approximation (MIA), leveraging Farkas' lemma to reformulate the problem as an LP. This method is widely used for its efficiency [5], [10]. Zhang et al. [10] further enhanced this method, establishing it as one of the state-of-the-art algorithms for approximating the Minkowski sum.

Received 19 May 2025; revised 28 October 2025; accepted 29 December 2025. Date of publication 5 January 2026; date of current version 23 April 2026. This work was supported in part by Data-Analytics for Enhanced Operation of Local Energy Systems from a Cyber-Physical-Social Perspectives (DATALESs) Project jointly funded by The Netherlands Organization for Scientific Research (NWO) and the National Natural Science Foundation of China (NSFC) under Grant 482.20.602, and in part by NSFC under Grant 52307103. Paper no. TSG-00961-2025. *(Corresponding author: Hongye Guo.)*

Chuyi Li, Kedi Zheng, Ning Zhang, and Hongye Guo are with the State Key Laboratory of Power System Operation and Control, Department of Electrical Engineering, Tsinghua University, Beijing 100084, China (e-mail: hyguo@tsinghua.edu.cn).

Pedro P. Vergara is with the Department of Electrical Sustainable Energy, Delft University of Technology, 2628 CD Delft, The Netherlands.

Digital Object Identifier 10.1109/TSG.2025.3650457

1949-3053 © 2026 IEEE. All rights reserved, including rights for text and data mining, and training of artificial intelligence and similar technologies. Personal use is permitted, but republication/redistribution requires IEEE permission.
See https://www.ieee.org/publications/rights/index.html for more information.

Authorized licensed use limited to: TU Delft Library. Downloaded on September 07,2026 at 09:48:45 UTC from IEEE Xplore. Restrictions apply.

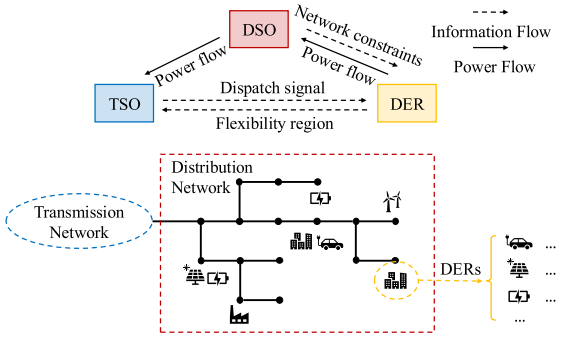


Fig. 1. Framework of interaction among TSO, DSO, and DER aggregator.

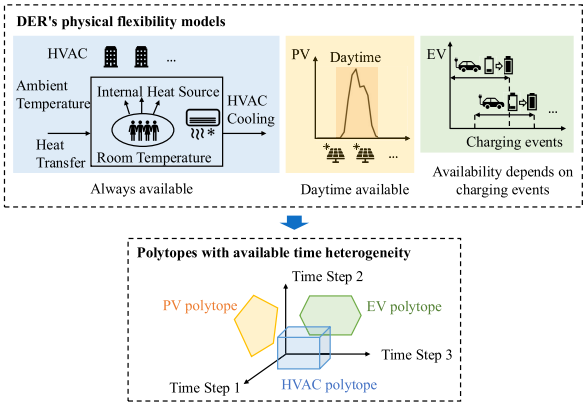


Fig. 2. Illustration of time heterogeneity. Time heterogeneity is reflected by polytopes that degenerate to different subspaces (bottom) due to varying availability durations (top).

Despite these advancements, several key challenges still exist for the Minkowski formulation. The first is time heterogeneity. DER models often involve different state variables and have distinct available time periods, resulting in polytopes of varying dimensions. Although state heterogeneity has been widely studied [11], time heterogeneity has received less attention. A recent study addressed the time heterogeneity of EVs through a case-specific projection process [10], but this method is difficult to generalize. The second challenge relates to network security. Since DERs are connected to the distribution network, the involvement of the distribution system operator (DSO) is essential to ensure secure operation. However, the Minkowski formulation is inherently incompatible with network models. A practical approach is to have the DSO impose node-specific net power limits, known as operating envelopes (OEs) [12], [13]. While effective, OEs decouple the network constraints, which introduces conservatism. The final challenge is error accumulation. In Minkowski-based aggregation, approximations must be performed repeatedly for individual DERs before aggregation. As the number of DERs increases, these approximation errors accumulate, and the resulting aggregated region may no longer serve as an MIA of the exact flexibility region.

The projection formulation provides a more general approach to aggregation by combining all individual models and eliminating undesired variables [7], [14], [15], [16]. It naturally accounts for both time heterogeneity and network constraints, directly yielding the aggregated result through projection MIA, thus avoiding error accumulation. However, this advantage comes with much higher computational complexity, since the projection formulation cannot aggregate DERs sequentially as in the Minkowski formulation. Instead, it results in a single large-scale problem. Consequently, large-scale aggregation using projection formulation requires special attention.

Even at the same problem scale, projection is usually more computationally demanding than the Minkowski sum. Classical exact algorithms, such as vertex enumeration, the double description method [17], and Fourier–Motzkin elimination [18], suffer from exponential or worse computational complexity. For practical computation, existing studies have adopted box [7] or ellipsoidal [14] approximations, formulating the problem as quadratic programming (QP) or semi-definite programming (SDP). In [15] and [16], a polytope outer approximation is first performed, followed by a bound-shrinking strategy to reduce overestimation, leading to a mixed-integer linear programming (MILP) formulation. To our knowledge, no LP-based method has been reported for solving projection MIA problems so far.

Meanwhile, most of the studies above assume that the DSO directly performs the aggregation. The DSO should instead act as a third-party entity responsible for enforcing network security constraints. How to develop a network constraint model, less conservative than OEs, that enables such coordination without disclosing sensitive network parameters needs further investigation.

B. Contribution

The comparative features of existing DER aggregation studies are summarized in Table I. To address the current research gap, this paper investigates the aggregation of large-scale DERs in distribution systems. We first establish a novel projection model to accommodate DER heterogeneity and develop an LP-based algorithm to solve the resulting standard projection MIA problem. A hierarchical aggregation framework is employed to ensure scalability, and a generalized OE is introduced to effectively incorporate network security constraints. This generalized OE can be enforced by the DSO and seamlessly integrated into the aggregation process, providing a practical mechanism for enabling TSO–DER interactions, as illustrated in Fig. 1.

The main contributions of this paper are as follows:

- A novel projection model is developed to aggregate multiple DERs while accommodating time heterogeneity. It is formulated as a standard projection problem, i.e., the dimension reduction of a polytope in half-space representation (H-representation), which provides a convenient form for approximation.
- An LP-based algorithm is developed to solve the standard projection MIA problem. To our knowledge, this is the first LP-based method for projection MIA, providing high computational efficiency while maintaining superior approximation accuracy.
- A hierarchical aggregation framework is designed for large-scale aggregation scenarios, and a Minkowski-closed family is proven, allowing accurate and efficient secondary aggregation through vector addition.

Authorized licensed use limited to: TU Delft Library. Downloaded on September 07,2026 at 09:48:45 UTC from IEEE Xplore. Restrictions apply.

- A generalized OE is introduced to model network security constraints. It captures nodal coupling and prevents disclosure of sensitive network information, allowing seamless integration into the aggregation model.

II. Heterogeneity of DER Models

The feasible region of the overall active power consumption of a DER represents its flexibility.[1] It is typically modeled by a set of equalities and inequalities, forming a high-dimensional polytope. Heterogeneous DERs are described by distinct state equations involving different internal state variables, resulting in state heterogeneity. Moreover, DERs are available for dispatch during different time periods, leading to time heterogeneity. In the following subsections, PVs, HVACs, and EVs are used as examples to illustrate the mathematical essence of these types of heterogeneity.

A. DERs With Heterogeneous States

PVs are the simplest type of DERs, having no internal state dynamics. Their behavior can be modeled as:

$$\underline{P}_t^{\mathrm{PV}} \le P_t^{\mathrm{PV}} < \overline{P}_t^{\mathrm{PV}},\ \tau^{\mathrm{start}} < t \le \tau^{\mathrm{end}} \tag{1}$$

where P^{PV} is the output power; overline ($\bar{\cdot}$) and underline ($\underline{\cdot}$) denote the upper and lower bounds; t is the time index; and $\tau^{\mathrm{start}} < t \le \tau^{\mathrm{end}}$ indicates the period when the PV is active.

Equation (1) defines a polytope in the space of overall power consumption. In matrix form, it can be expressed in standard H-representation as:

$$\boldsymbol{A}^{\mathrm{PV}}\boldsymbol{P}^{\mathrm{PV}} \le \boldsymbol{b}^{\mathrm{PV}},\ \boldsymbol{P}^{\mathrm{PV}} \in \mathbb{R}^{\tau^{\mathrm{end}}-\tau^{\mathrm{start}}} \tag{2}$$

For some DERs, modeling becomes more complex due to temporal coupling through internal states, resulting in state heterogeneity. For HVAC systems, the internal state is the room temperature. The model is described in [3]:

$$\underline{P}^{\mathrm{HVAC}} \le P_t^{\mathrm{HVAC}} < \overline{P}^{\mathrm{HVAC}},\ 0 \le t \le \tau \tag{3a}$$

$$T_t^{\mathrm{HVAC}} = \eta^{\mathrm{HVAC}} T_{t-1}^{\mathrm{HVAC}} + \Delta\tau\alpha^{\mathrm{HVAC}} P_t^{\mathrm{HVAC}} + (1-\eta^{\mathrm{HVAC}}) w_t^{\mathrm{HVAC}} \tag{3b}$$

$$\underline{T}^{\mathrm{HVAC}} \le T_t^{\mathrm{HVAC}} \le \overline{T}^{\mathrm{HVAC}} \tag{3c}$$

where P_t^{HVAC} and T_t^{HVAC} denote power consumption and room temperature, respectively; η^{HVAC} is the thermal dissipation rate; α^{HVAC} is the conversion factor from energy to temperature; w_t^{HVAC} is the ambient temperature; and $\Delta\tau$ is the time step. $0 \le t \le \tau$ indicates the full time availability.

[1] In some literature, the reactive flexibility of DERs is also included. In these models, the constraints introduced by reactive power control should also be considered. As summarized in [19], four typical control modes may apply: constant Q, constant power factor, P–Q control, and V–Q control, all of which can be represented in linear or piecewise-linear forms. In current system and market operations, the flexibility of reactive power is much less critical and less emphasized than that of active power. Therefore, this paper adopts the first mode, treating reactive power as a constant. It is worth noting, however, that adopting other control modes to explicitly model reactive power does not alter the polytope nature of the flexibility model, and the proposed method in this paper remains applicable.

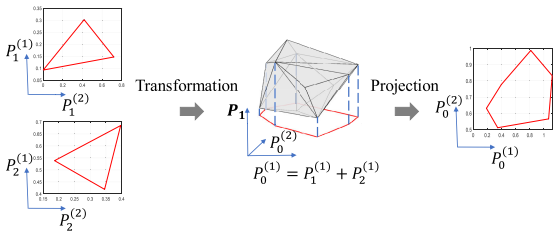


Fig. 3. Transformation and projection method for calculating the Minkowski sum of two polytopes. $\boldsymbol{P}_1$, $\boldsymbol{P}_2$, and $\boldsymbol{P}_0$ denote the dimensional variables of the two original polytopes and their aggregation, respectively. Superscripts (1) and (2) indicate vector indices.

According to [3], the state equation (3b) can be used to eliminate internal states, resulting in a standard polytope in the space of overall power consumption:

$$\boldsymbol{A}^{\mathrm{HVAC}}\boldsymbol{P}^{\mathrm{HVAC}} \le \boldsymbol{b}^{\mathrm{HVAC}},\ \boldsymbol{P}^{\mathrm{HVAC}} \in \mathbb{R}^{\tau} \tag{4}$$

Similar to the derivation for HVACs, a standard procedure is summarized in [11] to eliminate state heterogeneity among different DERs, thereby unifying their flexibility representations as H-represented polytopes in the space of interface power consumption across multiple time steps. The mathematical formulation is given as:

$$\boldsymbol{A}^{\mathrm{DER}}\boldsymbol{P}^{\mathrm{DER}} \le \boldsymbol{b}^{\mathrm{DER}},\ \boldsymbol{P}^{\mathrm{DER}} \in \mathbb{R}^{\tau^{\mathrm{DER}}} \tag{5}$$

B. DERs With Heterogeneous Available Time

While existing research has effectively addressed state heterogeneity, time heterogeneity remains less explored. DERs such as HVACs are available throughout the entire scheduling horizon, resulting in polytopes defined in full-dimensional spaces, as in (4). In contrast, DERs like PVs are only active during specific time periods, as in (2). These non-uniform availability windows cause the corresponding polytopes to degenerate into lower-dimensional subspaces, meaning that when plotted in the full scheduling horizon space, these degenerated polytopes, with only partial time availability, exhibit affine dimensions smaller than the space dimension, as shown in the lower part of Fig. 2.

EVs are another example of DERs with time heterogeneity. If we consider only EV charging events,[2] their models are as follows:

$$\underline{P}^{\mathrm{EV}} \le P_t^{\mathrm{EV}} \le \overline{P}^{\mathrm{EV}},\ \tau^{\mathrm{start}} < t \le \tau^{\mathrm{end}} \tag{6a}$$

$$E_t^{\mathrm{EV}} = \eta^{\mathrm{EV}} E_{t-1}^{\mathrm{EV}} + \Delta\tau\alpha^{\mathrm{EV}} P_t^{\mathrm{EV}} \tag{6b}$$

$$\underline{E}^{\mathrm{EV}} \le E_t^{\mathrm{EV}} \le \overline{E}^{\mathrm{EV}} \tag{6c}$$

$$E_{\tau^{\mathrm{end}}} \ge E^{\mathrm{end}} \tag{6d}$$

where P^{EV} and E^{EV} are the power and state-of-charge (SOC), respectively; η^{EV} denotes the self-discharge rate; α^{EV} denotes the charging efficiency; τ^{start} and τ^{end} specify the charging window; E^{end} is the target SOC; and $\Delta\tau$ is the time step.

After eliminating internal state variables as described in Section II-A, the resulting model becomes $\boldsymbol{A}^{\mathrm{EV}}\boldsymbol{P}^{\mathrm{EV}} \le \boldsymbol{b}^{\mathrm{EV}}$, where $\boldsymbol{P}^{\mathrm{EV}} \in \mathbb{R}^{\tau^{\mathrm{end}}-\tau^{\mathrm{start}}}$.

[2] Vehicle-to-Grid (V2G) technology enables EVs to sell electricity back to the grid. For simplicity, only charging events are considered in this paper.

Authorized licensed use limited to: TU Delft Library. Downloaded on September 07,2026 at 09:48:45 UTC from IEEE Xplore. Restrictions apply.

TABLE I
COMPARATIVE FEATURES OF EXISTING DER AGGREGATION STUDIES

Ref.	Aggregation Type	Optimization Method	Time Heterogeneity	Network Constraints	DSO Role
[3], [11]	Outer	LP	×	×	×
[4], [5], [8], [9]	Inner	LP, SDP	×	×	×
[10]	Inner	LP	✓	×	×
[12], [13]	×	×	✓	✓	Setting OE
[7], [14], [15], [16]	MIA	QP, SDP, MILP	✓	✓	Performing Aggregation
This work	MIA	LP	✓	✓	Setting Generalized OE

Remark 1: Some DERs may have multiple separate availability windows. For example, an EV charger provides flexibility only when an EV is connected. Since these windows do not overlap, a single DER can be represented as multiple distinct DERs, each corresponding to a continuous availability window. For EV chargers, each window corresponds to a charging event, serving as the smallest modeling unit for EVs in this paper.

Since there is no mathematical way to expand degenerated polytopes into full-dimensional spaces, time heterogeneity cannot be eliminated like state heterogeneity. This issue has received limited attention, as most Minkowski formulations are designed for non-degenerated polytopes, making them unsuitable for degenerated cases. To address this limitation, the next section introduces a novel projection formulation that accommodates time heterogeneity.

III. PROJECTION FORMULATION OF DER AGGREGATION

Ignoring network constraints, the aggregation of DERs simplifies to calculating the Minkowski sum of polytopes. Let the pair $(\boldsymbol{A}, \boldsymbol{b})$ represent a polytope defined by $\boldsymbol{AP} \le \boldsymbol{b}$. For two such polytopes, $(\boldsymbol{A}_1, \boldsymbol{b_1})$ and $(\boldsymbol{A}_2, \boldsymbol{b_2})$, their Minkowski sum is defined as:

$$(\boldsymbol{A}_1, \boldsymbol{b_1}) \oplus (\boldsymbol{A}_2, \boldsymbol{b}_2) = \left\{ \boldsymbol{P}_0 \,\middle|\, \begin{array}{c} \boldsymbol{P}_0 = \boldsymbol{P}_1 + \boldsymbol{P}_2 \\ \boldsymbol{A}_1\boldsymbol{P}_1 \le \boldsymbol{b}_1, \boldsymbol{A}_2\boldsymbol{P}_2 \le \boldsymbol{b}_2 \end{array} \right\} \tag{7}$$

The method proposed in [11] provides a standard procedure to address this problem, as illustrated in Fig. 3. The left part of the figure shows the Minkowski sum of two polytopes, corresponding to (7). From a polytope projection perspective, this operation can be reformulated as:

$$\left\{ \boldsymbol{P}_0 \,\middle|\, \begin{array}{l} \begin{bmatrix} -\boldsymbol{I} & -\boldsymbol{I} & \boldsymbol{I} \end{bmatrix} \begin{bmatrix} \boldsymbol{P}_1 \\ \boldsymbol{P}_2 \\ \boldsymbol{P}_0 \end{bmatrix} = \boldsymbol{0} \\ \begin{bmatrix} \boldsymbol{A}_1 & \boldsymbol{0} \\ \boldsymbol{0} & \boldsymbol{A}_2 \end{bmatrix} \begin{bmatrix} \boldsymbol{P}_1 \\ \boldsymbol{P}_2 \end{bmatrix} \le \begin{bmatrix} \boldsymbol{b_1} \\ \boldsymbol{b_2} \end{bmatrix} \end{array} \right\} \tag{8}$$

This reformulation describes the projection of a polytope defined by both equality and inequality constraints. Since this form is not in standard H-representation, it complicates the projection process. According to Proposition 1 in [11], a transformation matrix $\boldsymbol{W}$ can be constructed to make the problem equivalent to the dimension reduction of an H-represented polytope, referred to as a standard projection, as follows:

$$\left\{ \boldsymbol{P}_0 \,\middle|\, \begin{bmatrix} \boldsymbol{A}_1 & \boldsymbol{0} \\ \boldsymbol{0} & \boldsymbol{A}_2 \end{bmatrix} \boldsymbol{W}^{-1} \begin{bmatrix} \boldsymbol{x}' \\ \boldsymbol{P}_0 \end{bmatrix} \le \begin{bmatrix} \boldsymbol{b_1} \\ \boldsymbol{b_2} \end{bmatrix} \right\} \tag{9}$$

In this specific case, the transformation matrix is given as $\boldsymbol{W} = \begin{bmatrix} \boldsymbol{I} & \boldsymbol{0} \\ \boldsymbol{I} & \boldsymbol{I} \end{bmatrix}$, with the dimensions to be reduced given by $\boldsymbol{x}' = \boldsymbol{P}_1$. The middle part of Fig. 3 illustrates this transformation equivalence.

In the original formulation (7), the problem involves projecting a degenerate polytope from a 3τ-D space to a τ-D space. The standard form (9) instead projects an H-represented polytope from a 2τ-D space to a τ-D space, thereby greatly simplifying the computation.

The above derivation can be naturally extended to the aggregation of multiple polytopes. To accommodate time heterogeneity, equation (8) is further extended to handle the Minkowski sum of degenerate polytopes:

$$\left\{ \boldsymbol{P}_0 \,\middle|\, \begin{array}{l} \left[\cdots \quad -\boldsymbol{M}_k \quad \cdots \middle| \quad \boldsymbol{I} \right] \begin{bmatrix} \vdots \\ \boldsymbol{P}_k \\ \vdots \\ \hline \boldsymbol{P}_0 \end{bmatrix} = \boldsymbol{0}, k \in \mathcal{K} \\ \begin{bmatrix} \ddots & & \\ & \boldsymbol{A}_k & \\ & & \ddots \end{bmatrix} \begin{bmatrix} \vdots \\ \boldsymbol{P}_k \\ \vdots \end{bmatrix} \le \begin{bmatrix} \vdots \\ \boldsymbol{b}_k \\ \vdots \end{bmatrix} \end{array} \right\} \tag{10a}$$

$$\boldsymbol{M}_k = \begin{bmatrix} \boldsymbol{0}_{d_k \times m_{k_1}} & \boldsymbol{I}_{d_k \times d_k} & \boldsymbol{0}_{d_k \times m_{k_2}} \end{bmatrix}^\top \tag{10b}$$

where $\mathcal{K}$ is the index set for DERs; d_k is the number of time steps during which DERk is available; and m_{k_1} and m_{k_2} denote the durations before and after its availability, respectively. When the DER is available throughout the entire horizon, $\boldsymbol{M}_k = \boldsymbol{I}$. Similarly, there exists a transformation matrix $\boldsymbol{W}$ such that:

$$(10) \Leftrightarrow \left\{ \boldsymbol{P}_0 \,\middle|\, \begin{bmatrix} \ddots & & \\ & \boldsymbol{A}_k & \\ & & \ddots \end{bmatrix} \boldsymbol{W}^{-1} \begin{bmatrix} \boldsymbol{x}' \\ \boldsymbol{P}_0 \end{bmatrix} \le \begin{bmatrix} \vdots \\ \boldsymbol{b}_k \\ \vdots \end{bmatrix} \right\} \tag{11}$$

Authorized licensed use limited to: TU Delft Library. Downloaded on September 07,2026 at 09:48:45 UTC from IEEE Xplore. Restrictions apply.

Naturally, the projection of a polytope remains a polytope and can be represented in H-representation. We define a mapping to denote the standard projection operation as:

$$Proj : (\boldsymbol{A}, \boldsymbol{b}; \boldsymbol{y}) \rightarrow \left(\boldsymbol{A}', \boldsymbol{b}'\right) \tag{12}$$

where $(\boldsymbol{A}, \boldsymbol{b})$ and $(\boldsymbol{A}', \boldsymbol{b}')$ are the original and projected polytopes, respectively, and $\boldsymbol{y}$ denotes the variables to be preserved during projection. Accordingly, equation (10) can be reformulated as:

$$Proj\left(\begin{bmatrix} \ddots & & \\ & \boldsymbol{A}_k & \\ & & \ddots \end{bmatrix} \boldsymbol{W}^{-1}, \begin{bmatrix} \vdots \\ \boldsymbol{b}_k \\ \vdots \end{bmatrix}; \boldsymbol{P}_0\right) \tag{13}$$

Equation (13) presents a standard projection formulation for aggregating multiple DERs. It naturally accommodates time heterogeneity and avoids the repeated approximations in sequential Minkowski sums. While the aggregation problem remains challenging, it is now equivalent to a standard projection approximation problem. In the next section, we introduce an efficient and accurate algorithm to solve this problem.

IV. An LP-Based Algorithm to Solve Projection MIA Problem

A. Projection MIA Problem Formulation

A projection problem as follows is studied in this section. For the polytope $\begin{bmatrix} \boldsymbol{A} & \boldsymbol{B} \end{bmatrix} \begin{bmatrix} \boldsymbol{x} \\ \boldsymbol{y} \end{bmatrix} \leq \boldsymbol{d}$, the operation reducing $\boldsymbol{x}$ is given by:

$$Proj\left([\boldsymbol{A}, \boldsymbol{B}], \boldsymbol{d}; \boldsymbol{y}\right) \tag{14}$$

It has been recognized that obtaining the exact result of (14) is computationally intractable in practice [20]. Existing research has suggested that, in the context of DER flexibility modeling, inner approximations are generally preferable, as overestimation may lead to infeasible dispatch decisions. A commonly adopted strategy is to adjust a given prototype polytope $(\boldsymbol{\Gamma}, \boldsymbol{\gamma})$ to inscribe the exact feasible set. Let β and $\boldsymbol{\upsilon}$ denote the scaling and translation parameters, the adjusted polytope is then represented as $(\boldsymbol{\Gamma}, \boldsymbol{\gamma}')$, where

$$\boldsymbol{\gamma}' = \beta\boldsymbol{\gamma} + \boldsymbol{\Gamma}\boldsymbol{\upsilon} \tag{15}$$

All possible polytopes $(\boldsymbol{\Gamma}, \boldsymbol{\gamma}')$ corresponding to different values of $\boldsymbol{\gamma}'$ are referred to as homothets, as they can be generated by scaling and translating a common prototype polytope. Using the concept of homothets, the inner approximation can be formulated as:

$$\begin{aligned} &\max_{\beta, \boldsymbol{\upsilon}} \beta \\ &\text{s.t.:} \quad (\boldsymbol{\Gamma}, \boldsymbol{\gamma}') \subseteq proj([\boldsymbol{A}, \boldsymbol{B}], \boldsymbol{d}; \boldsymbol{y}) \end{aligned} \tag{16}$$

This problem aims to maximize the approximation of a projection and is called a projection MIA problem. While polytope MIA problems have been effectively addressed using Farkas' lemma [9], projection MIAs are generally considered more difficult. In the following subsections, we show that the projection MIA problem can be efficiently solved with an LP formulation.

B. LP-Based Method for Solving MIA

Before performing the approximation, a prototype polytope must be selected to derive homothets. There are various options, such as using virtual generators (VGs) or virtual batteries (VBs) [15]. In this paper, we choose a VB model with ramping limits, which corresponds to a prototype polytope with a left-hand-side (LHS) matrix:

$$\boldsymbol{\Gamma} = [\boldsymbol{G}, -\boldsymbol{G}]^\top \tag{17a}$$

$$\boldsymbol{G} = \begin{bmatrix} 1 & 1 & \dots & 1 & 1 & & & 1 & & \\ & 1 & \dots & 1 & -1 & \ddots & & & 1 & \\ & & \ddots & \vdots & & \ddots & 1 & & & \ddots \\ & & & 1 & & & -1 & & & 1 \end{bmatrix} \tag{17b}$$

and the right-hand-side (RHS) vector $\boldsymbol{\gamma}$ is obtained by constructing an outer approximation using LP as follows:

$$\begin{aligned} \gamma_i = \max_{\boldsymbol{x}, \boldsymbol{y}} \boldsymbol{\Gamma}_i \boldsymbol{y}, \ i \in \mathcal{I} \\ \text{s.t.:} \quad \begin{bmatrix} \boldsymbol{A} & \boldsymbol{B} \end{bmatrix} \begin{bmatrix} \boldsymbol{x} \\ \boldsymbol{y} \end{bmatrix} \leq \boldsymbol{d} \end{aligned} \tag{18}$$

where $\mathcal{I}$ is the set of $\boldsymbol{\Gamma}$ row indices.

By adopting the concept of robust optimization modeling and using the definition of projection, problem (16) can be reformulated as:

$$\begin{aligned} &\max_{\boldsymbol{x}^{(j)}, \boldsymbol{y}^{(j)}, \boldsymbol{\upsilon}, \beta > 0} \beta \\ &\text{s.t.:} \quad \left(\min_{[\boldsymbol{x}^{(j)}; \boldsymbol{y}^{(j)}] \in \Omega_1} \left(\boldsymbol{a}_j \boldsymbol{x}^{(j)} + \max_{\boldsymbol{y}^{(j)} \in \Omega_2} \boldsymbol{b}_j \boldsymbol{y}^{(j)}\right)\right) \leq d_j, \\ &\quad j \in \mathcal{J} \end{aligned} \tag{19}$$

where $\mathcal{J}$ denotes the set of row indices; Ω_1 and Ω_2 represent the original polytope and its approximated projection, respectively:

$$\Omega_1 = \left\{ \begin{bmatrix} \boldsymbol{x} \\ \boldsymbol{y} \end{bmatrix} \middle| \begin{bmatrix} \boldsymbol{A} & \boldsymbol{B} \end{bmatrix} \begin{bmatrix} \boldsymbol{x} \\ \boldsymbol{y} \end{bmatrix} \leq \boldsymbol{d} \right\} \tag{20a}$$

$$\Omega_2 = \left\{ \boldsymbol{y} \middle| \boldsymbol{\Gamma}\boldsymbol{y} \leq \boldsymbol{\gamma}' \right\} \tag{20b}$$

According to the projection operation in problem (16), for any point $\boldsymbol{y}^{(j)}$ in the approximated projection Ω_2, it should be possible to find a corresponding point $\begin{bmatrix} \boldsymbol{x}^{(j)} \\ \boldsymbol{y}^{(j)} \end{bmatrix}$ lying inside the original polytope Ω_1. To ensure this, in (19) the choice of $\boldsymbol{y}^{(j)}$ is made to maximize the term $\boldsymbol{b}_j \boldsymbol{y}^{(j)}$, representing the worst case for satisfying the jth polytope constraint $\boldsymbol{a}_j \boldsymbol{x}^{(j)} + \boldsymbol{b}_j \boldsymbol{y}^{(j)} \leq d_j$. If such a $\boldsymbol{x}^{(j)}$ exists for every constraint $j \in \mathcal{J}$, then Ω_2 is guaranteed to be contained within the projection of Ω_1, as illustrated in Fig. 4. Maximizing the scaling factor β thus yields the projection MIA, equivalent to problem (16).

To solve (19), we replace the inner maximization $\max_{\boldsymbol{y}^{(j)} \in \Omega_2} \boldsymbol{b}_j \boldsymbol{y}^{(j)}$ with its dual using the duality theorem and merge the two minimizations, reformulating the problem as:

$$\max_{\boldsymbol{x}^{(j)}, \boldsymbol{y}^{(j)}, \boldsymbol{\upsilon}, \beta > 0} \beta \tag{21a}$$

$$\text{s.t.:} \quad \min_{\substack{[\boldsymbol{x}^{(j)}; \boldsymbol{y}^{(j)}] \in \Omega_1 \\ \boldsymbol{\omega}_j \in \Omega_3^{(j)}}} \left(\boldsymbol{a}_j \boldsymbol{x}^{(j)} + \boldsymbol{\omega}_j^\top (\beta\boldsymbol{\gamma} + \boldsymbol{\Gamma}\boldsymbol{\upsilon})\right) \leq d_j,$$

Authorized licensed use limited to: TU Delft Library. Downloaded on September 07,2026 at 09:48:45 UTC from IEEE Xplore. Restrictions apply.

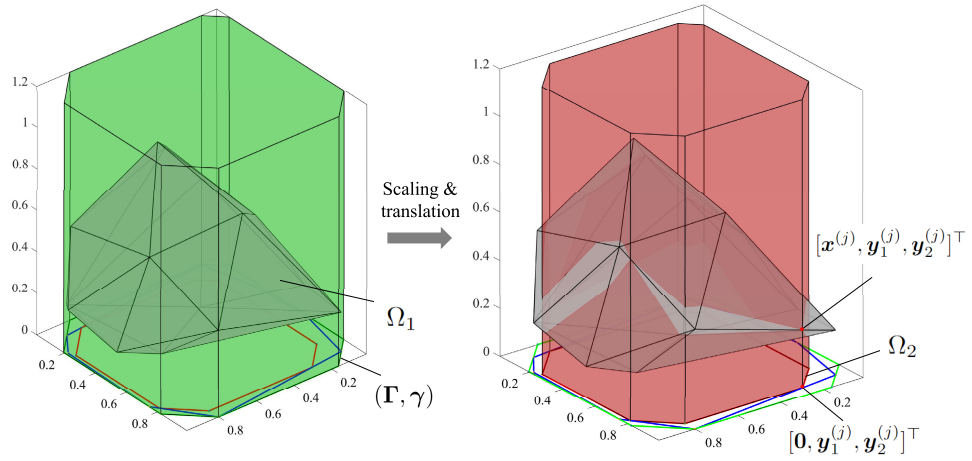


Fig. 4. Illustration of the projection MIA modeling. The gray polytope represents the original polytope to be projected. The green polytope represents the initial outer approximation, which is scaled and translated to form the red MIA.

$$j \in \mathcal{J} \tag{21b}$$

$$\boldsymbol{b}_j \boldsymbol{y}^{(j)} = \boldsymbol{\omega}_j^\top (\beta \boldsymbol{\gamma} + \boldsymbol{\Gamma} \boldsymbol{\upsilon}), \ \ j \in \mathcal{J} \tag{21c}$$

$$\boldsymbol{\Gamma} \boldsymbol{y}^{(j)} \le \beta \boldsymbol{\gamma} + \boldsymbol{\Gamma} \boldsymbol{\upsilon}, \ \ j \in \mathcal{J} \tag{21d}$$

where $\boldsymbol{\omega}_j$ are the dual variables and $\Omega_3^{(j)} = \left\{\boldsymbol{\omega} \mid \boldsymbol{\omega}^\top \boldsymbol{\Gamma} = \boldsymbol{b}_j, \ \boldsymbol{\omega} \ge \boldsymbol{0}\right\}$ is the feasible set of the dual problem. Because the dual formulation does not explicitly provide the value of $\boldsymbol{y}^{(j)}$, the KKT conditions (21c)–(21d) are incorporated to ensure equivalence, yielding $\boldsymbol{y}^{(j)}$ corresponding to each $\boldsymbol{\omega}_j$.

The minimization in (21b) can be removed without changing the problem, and (21c) can be used to simplify (21b), leading to a set of constraints that partially overlap with those defining Ω_1. Let $\boldsymbol{W} = \left[\dots \ \boldsymbol{\omega} j \ \dots \right]^\top$, and the problem can be compactly expressed as:

$$\begin{aligned} \max_{\boldsymbol{x}^{(j)}, \boldsymbol{y}^{(j)}, \boldsymbol{\upsilon}, \boldsymbol{W} \ge \boldsymbol{0}, \beta > 0} \ & \beta \\ \text{s.t.:} \ \ & \boldsymbol{A}\boldsymbol{x}^{(j)} + \boldsymbol{B}\boldsymbol{y}^{(j)} \le \boldsymbol{d}, \ \ j \in \mathcal{J} \\ & \boldsymbol{b}_j \boldsymbol{y}^{(j)} = \boldsymbol{\omega}_j^\top (\beta \boldsymbol{\gamma} + \boldsymbol{\Gamma} \boldsymbol{\upsilon}), \ \ j \in \mathcal{J} \\ & \boldsymbol{\Gamma} \boldsymbol{y}^{(j)} \le \beta \boldsymbol{\gamma} + \boldsymbol{\Gamma} \boldsymbol{\upsilon}, \ \ j \in \mathcal{J} \\ & \boldsymbol{W}\boldsymbol{\Gamma} = \boldsymbol{B} \end{aligned} \tag{22}$$

Due to the complementary relaxation condition, the bilinear term $\boldsymbol{\omega}_j^\top (\beta \boldsymbol{\gamma} + \boldsymbol{\Gamma} \boldsymbol{\upsilon})$ is introduced. Fortunately, since β always has a positive value, a substitution can be made to linearize the problem, resulting in an equivalent form:

$$\begin{aligned} \min_{\boldsymbol{x}^{(j)'}, \boldsymbol{y}^{(j)'}, \boldsymbol{\upsilon}', \boldsymbol{W} \ge \boldsymbol{0}, \beta' > 0} \ & \beta' \\ \text{s.t.:} \ \ & \boldsymbol{A}\boldsymbol{x}^{(j)'} + \boldsymbol{B}\boldsymbol{y}^{(j)'} \le \beta' \boldsymbol{d}, \ \ j \in \mathcal{J} \\ & \boldsymbol{b}_j \boldsymbol{y}^{(j)'} = \boldsymbol{\omega}_j^\top \boldsymbol{\gamma} + \boldsymbol{b}_j \boldsymbol{\upsilon}', \ \ j \in \mathcal{J} \\ & \boldsymbol{\Gamma} \boldsymbol{y}^{(j)'} \le \boldsymbol{\gamma} + \boldsymbol{\Gamma} \boldsymbol{\upsilon}', \ \ j \in \mathcal{J} \\ & \boldsymbol{W}\boldsymbol{\Gamma} = \boldsymbol{B} \end{aligned} \tag{23}$$

where

$$\beta' = \frac{1}{\beta}, \ \ \boldsymbol{x}^{(j)'} = \frac{\boldsymbol{x}^{(j)}}{\beta}, \ \ \boldsymbol{y}^{(j)'} = \frac{\boldsymbol{y}^{(j)}}{\beta}, \ \ \boldsymbol{\upsilon}' = \frac{\boldsymbol{\upsilon}}{\beta} \tag{24}$$

Problem (23) presents an LP for solving the projection MIA problem, which is summarized in **Algorithm 1**.

Algorithm 1 LP-Based Projection MIA

1: **Input:** Original polytope $([\boldsymbol{A}, \boldsymbol{B}], \boldsymbol{d})$;
2: **Output:** Approximated projection $(\boldsymbol{\Gamma}, \boldsymbol{\gamma}')$;
3: Construct matrix $\boldsymbol{\Gamma}$;
4: **for** $i \in \mathcal{I}$ **do**
5: Solve LP (18) to get γ_i;
6: **end for**
7: Solve LP (23) to get $\beta', \boldsymbol{\upsilon}'$;
8: Restore $\beta, \boldsymbol{\upsilon}$ according to (24);
9: $\boldsymbol{\gamma}' \leftarrow \beta \boldsymbol{\gamma} + \boldsymbol{\Gamma} \boldsymbol{\upsilon}$;
10: **Return** $(\boldsymbol{\Gamma}, \boldsymbol{\gamma}')$

V. System-Level Large-Scale Aggregation

Adopting **Algorithm 1** proposed in Section IV, the problem of aggregating multiple DERs, formulated as (13), can be efficiently solved. However, the number of constraints in the corresponding LP increases quadratically with the number of DERs. In large-scale aggregation scenarios, even the LP-based algorithm becomes less efficient. Additionally, for system-level aggregation, network constraints must be integrated into the model. To address these challenges, a hierarchical aggregation framework, as shown in Fig. 5, is proposed.

A. Aggregation by Clusters

In the first stage, marked by the yellow box in Fig. 5, DERs connected to the same node in the distribution network are considered. Aggregation at this stage can be performed without incorporating network constraints. When the number of DERs is small, all DERs at a node can be aggregated through a single projection. However, this becomes impractical in large-scale scenarios. To manage computational complexity, DERs at each node are divided into clusters, each containing a limited number of DERs. Aggregation is then performed within each cluster using the proposed method, a process called primary aggregation. The resulting approximation error depends on the number of clusters. Previous studies have shown that, by adopting suitably designed clustering methods, i.e., the Ng–Jordan–Weiss (NJW) spectral clustering used in [5], the approximation error can be effectively reduced.

Authorized licensed use limited to: TU Delft Library. Downloaded on September 07,2026 at 09:48:45 UTC from IEEE Xplore. Restrictions apply.

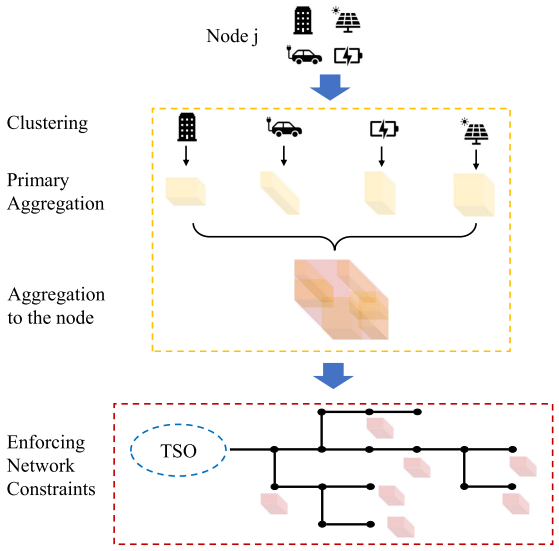


Fig. 5. Hierarchical aggregation framework: primary aggregation, secondary aggregation (aggregation to the node), and enforcing network constraints.

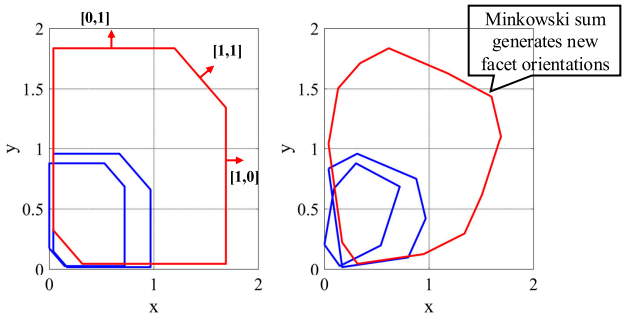


Fig. 6. Illustration of a Minkowski-closed family (left) and a non-Minkowski-closed family (right).

The outputs from the primary aggregation are then aggregated in the secondary aggregation stage. This process can potentially accumulate approximation errors and increase computation time. However, if each group of DERs in the primary aggregation includes at least one DER available at every time period, the polytopes resulting from the primary aggregation are no longer influenced by time heterogeneity. Furthermore, these polytopes are approximated using corresponding homothets, whose prototype polytopes share the same LHS matrix as in (17). Intuitively, they exhibit similar shapes, and the following proposition shows that their Minkowski sum can be efficiently obtained.

Proposition 1 (Minkowski-Closed Family): Consider a family of polytopes with an identical LHS matrix:

$$\Omega(\boldsymbol{b}^{(k)}) = (\boldsymbol{A}, \boldsymbol{b}^{(k)}) \tag{25}$$

For any two RHS vectors $\boldsymbol{b}^{(1)}$ and $\boldsymbol{b}^{(2)}$, the following inclusion always holds:

$$\Omega(\boldsymbol{b}^{(1)}) \oplus \Omega(\boldsymbol{b}^{(2)}) \subseteq \Omega(\boldsymbol{b}^{(1)} + \boldsymbol{b}^{(2)}) \tag{26}$$

Moreover, equality holds:

$$\Omega(\boldsymbol{b}^{(1)}) \oplus \Omega(\boldsymbol{b}^{(2)}) = \Omega(\boldsymbol{b}^{(1)} + \boldsymbol{b}^{(2)}) \tag{27}$$

if both polytopes are in minimal H-representation, that is:

$$\max_{\boldsymbol{x}\in\Omega(\boldsymbol{b}^{(k)})} \boldsymbol{a}_i\boldsymbol{x} = b_i^{(k)}, \quad \forall i \in \mathcal{I},\ k \in \{1,2\} \tag{28}$$

Proof: The inclusion result has been proved in Proposition 1 of [3].

Let $h_\Omega(\boldsymbol{u}) = \max_{\boldsymbol{x}\in\Omega} \boldsymbol{u}^\top \boldsymbol{x}$ denote the support function of Ω. It is known that for convex sets, $h_{\Omega_1\oplus\Omega_2}(\boldsymbol{u}) = h_{\Omega_1}(\boldsymbol{u}) + h_{\Omega_2}(\boldsymbol{u})$ [21]. For a polytope $\Omega(\boldsymbol{b}^{(k)})$, we have $h_{\Omega(\boldsymbol{b}^{(k)})}(\boldsymbol{a}_i) \le b_i^{(k)}$, with equality when the inequality $\boldsymbol{a}_i\boldsymbol{x} \le b_i^{(k)}$ is non-redundant. For polytopes in minimal H-representation, equality holds for all $i \in \mathcal{I}$. Hence:

$$h_{\Omega(\boldsymbol{b}^{(1)})\oplus\Omega(\boldsymbol{b}^{(2)})}(\boldsymbol{a}_i) = b_i^{(1)} + b_i^{(2)} = h_{\Omega(\boldsymbol{b}^{(1)}+\boldsymbol{b}^{(2)})}(\boldsymbol{a}_i)$$

Since two polytopes coincide if their support functions agree in all relevant directions [21], equality (27) holds.□

This proposition describes a family of polytopes whose Minkowski sum does not produce new facet orientations. This property is referred to as Minkowski-closed, as illustrated in Fig. 6. Since the polytopes obtained from the primary aggregation share the same LHS matrix, and the construction of homothets guarantees a minimal H-representation, the secondary aggregation can be significantly simplified according to **Proposition 1**, requiring only vector addition. This ensures high computational efficiency while maintaining accurate approximations.

Remark 2: Each constraint of the prototype polytope constructed by the outer approximation usually defines a valid facet orientation, as do the corresponding homothets. However, for certain DERs like PVs, which have relatively simple polytope shapes, some constraints, though capable of reaching equality, are tangent to the prototype polytope and do not define actual facet orientations. In such cases, numerical implementation can cause the resulting aggregated polytope to slightly extend beyond its true feasible boundary. This explains the occasional infeasibility of disaggregation observed in the case study presented later.

B. Enforcing Network Constraints

To characterize system-level flexibility for coordination with the TSO, the DSO must enforce network constraints during the aggregation process. In this context, the aggregation of DERs extends beyond the Minkowski sum of polytopes to incorporate coupling introduced by network physics. To model the network security constraints, the LinDistFlow model is adopted [22]:

$$p_j = \sum_{k:j\to k} P_{jk} - \sum_{i:i\to j} P_{ij}, \quad \forall j \in \mathcal{N} \tag{29a}$$

$$q_j = \sum_{k:j\to k} Q_{jk} - \sum_{i:i\to j} Q_{ij}, \quad \forall j \in \mathcal{N} \tag{29b}$$

$$v_j = v_i - 2\left(r_{ij}P_{ij} + x_{ij}Q_{ij}\right), \quad \forall (i,j) \in \mathcal{E} \tag{29c}$$

$$\underline{v_j} \le v_j \le \overline{v_j}, \quad \forall j \in \mathcal{N} \tag{29d}$$

where r and x are the branch resistance and reactance; v is the squared magnitudes of node voltage; $\mathcal{N}$ and $\mathcal{E}$ are the sets of nodes and branches; the time index t is omitted.

For (29a) and (29b), the path-branch incidence matrix $\boldsymbol{F}$ is adopted to formulate the topology of the network.

Authorized licensed use limited to: TU Delft Library. Downloaded on September 07,2026 at 09:48:45 UTC from IEEE Xplore. Restrictions apply.

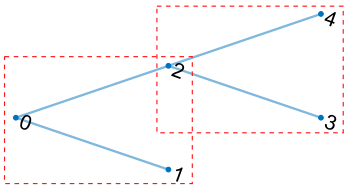


Fig. 7. Topology of the example network, where red boxes indicate a partition scheme.

The coupling between power injection and branch power is reformulated in matrix form:

$$\boldsymbol{P}_b = -\boldsymbol{F}^\top \boldsymbol{P}_N,\ \boldsymbol{Q}_b = -\boldsymbol{F}^\top \boldsymbol{Q}_N \Rightarrow \boldsymbol{S}_b = -\boldsymbol{F}'\boldsymbol{S}_N \tag{30}$$

where $\boldsymbol{S}_b = \left[\boldsymbol{P}_b, \boldsymbol{Q}_b\right]^\top = \left[\ldots, P_{ij}, \ldots, Q_{ij}, \ldots\right]^\top$; $\boldsymbol{S}_N = \left[\boldsymbol{P}_N, \boldsymbol{Q}_N\right]^\top = \left[\ldots, p_j, \ldots, q_j, \ldots\right]^\top$. Here, we use the example network illustrated in Fig. 7 for demonstration. The corresponding path-branch incidence matrix is as follows:

$$\boldsymbol{F} = \begin{bmatrix} 1 & 0 & 0 & 0 \\ 0 & 1 & 0 & 0 \\ 0 & 1 & 1 & 0 \\ 0 & 1 & 0 & 1 \end{bmatrix} \tag{31}$$

For (29c), in matrix form:

$$\begin{aligned} \boldsymbol{v}_N &= \boldsymbol{V}_0 + \boldsymbol{H}\boldsymbol{v}_N - 2\boldsymbol{r}_b\boldsymbol{P}_b - 2\boldsymbol{x}_b\boldsymbol{Q}_b \\ &\Leftrightarrow (\boldsymbol{I} - \boldsymbol{H})\,\boldsymbol{v}_N = \boldsymbol{V}_0 - 2\boldsymbol{z}_b\boldsymbol{S}_b \end{aligned} \tag{32}$$

where $\boldsymbol{v}_N = \left[\ldots, v_j, \ldots\right]^\top$; $\boldsymbol{z}_b = \left[diag(r_{ij}), diag(x_{ij})\right]$; term $(\boldsymbol{V}_0 + \boldsymbol{H}\boldsymbol{v}_N)$ represents $[\ldots, v_i, \ldots]^\top$. For the example network:

$$\boldsymbol{V}_0 = \begin{bmatrix} v_0 \\ v_0 \\ 0 \\ 0 \end{bmatrix},\ \boldsymbol{H} = \begin{bmatrix} 0 & 0 & 0 & 0 \\ 0 & 0 & 0 & 0 \\ 0 & 1 & 0 & 0 \\ 0 & 1 & 0 & 0 \end{bmatrix} \tag{33}$$

The construction of $\boldsymbol{H}$ guaranteed that it is a lower triangular matrix with zero main diagonal entries. Thus $(\boldsymbol{I} - \boldsymbol{H})$ must be invertible. Then utilizing (30):

$$\begin{aligned} \boldsymbol{v}_N &= (\boldsymbol{I} - \boldsymbol{H})^{-1}\,\boldsymbol{V}_0 - 2\,(\boldsymbol{I} - \boldsymbol{H})^{-1}\,\boldsymbol{z}_b\boldsymbol{S}_b \\ &= (\boldsymbol{I} - \boldsymbol{H})^{-1}\,\boldsymbol{V}_0 + 2\,(\boldsymbol{I} - \boldsymbol{H})^{-1}\,\boldsymbol{z}_b\boldsymbol{F}'\boldsymbol{S}_N \end{aligned} \tag{34}$$

Since this paper focuses on active power flexibility, reactive power is treated as a constant evaluated under the baseline load condition and is directly eliminated from the formulation, as is the active power injection at nodes without flexibility. By concentrating solely on flexible nodes and enforcing nodal voltage constraints, the network security constraints derived from the LinDistFlow model (29) can be reformulated as:

$$\boldsymbol{A}_t^{\text{sys}}\boldsymbol{P}_t \le \boldsymbol{b}_t^{\text{sys}} \tag{35}$$

Unlike conventional OEs, which only specify independent upper and lower bounds at individual nodes, constraint (35) defines a polytope in the multi-node power injection space. This polytope conveys richer information for DER aggregation while ensuring network security. Moreover, the pair $(\boldsymbol{A}_t^{\text{sys}}, \boldsymbol{b}_t^{\text{sys}})$ does not disclose sensitive network data, enhancing practical applicability. This form of constraint, referred to as a generalized OE, offers improved accuracy compared with conventional OEs.

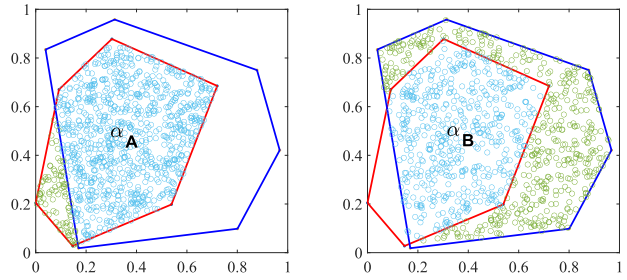


Fig. 8. Sampling-based method for calculating GMVR. An equal number of points are sampled from polytope A (red) and polytope B (blue). The number of points that lie in both polytopes, highlighted in blue, are α_A and α_B, respectively.

Since branch losses are neglected in the LinDistFlow model, the aggregation problem can be formulated similarly to (10), with additional constraints:

$$\left\{ \boldsymbol{p}_0 \;\middle|\; \begin{array}{l} \begin{bmatrix} \ldots & -\boldsymbol{M}_k & \ldots \end{bmatrix} \begin{bmatrix} \boldsymbol{I} \end{bmatrix} \begin{bmatrix} \vdots \\ \boldsymbol{P}_k \\ \vdots \\ \boldsymbol{p}_0 \end{bmatrix} = \boldsymbol{0},\ j \in \mathcal{K} \\ \begin{bmatrix} \ddots & & \\ & \boldsymbol{A}_k^{\text{agg}} & \\ & & \ddots \\ \ldots & \boldsymbol{A}_k^{\text{sys}} & \ldots \end{bmatrix} \begin{bmatrix} \vdots \\ \boldsymbol{P}_k \\ \vdots \end{bmatrix} \le \begin{bmatrix} \vdots \\ \boldsymbol{b}_k^{\text{agg}} \\ \vdots \\ \boldsymbol{b}^{\text{sys}} \end{bmatrix} \end{array} \right\} \tag{36}$$

where $\boldsymbol{p}_0$ is the root node power injection; $\left(\boldsymbol{A}_k^{\text{agg}}, \boldsymbol{b}_k^{\text{agg}}\right)$ is the aggregated polytope at node k; $\left(\boldsymbol{A}^{\text{sys}}, \boldsymbol{b}^{\text{sys}}\right)$ is give by the temporal expansion of (35).

When the aggregation scale becomes large, the radial network can be partitioned, illustrated by the red box in Fig. 7, and generalized OEs can be established for each sub-network separately. Each sub-network can then be aggregated individually, followed by a secondary aggregation step. This process is similar to the hierarchical framework shown in Fig. 5. It is worth noting that various partitioning schemes can be applied, but identifying the optimal partitioning strategy is beyond the scope of this paper.

VI. Case Study

A. Experimental Settings

In this section, numerical tests are conducted to evaluate the method proposed in this paper. The models and algorithms are implemented in MATLAB and solved with GUROBI. The computations are carried out on a desktop with an Intel i7 CPU and 16 GB of memory.

B. Metric

Approximation algorithms for the Minkowski sum or projection introduce errors, making performance evaluation essential. One aspect is flexibility coverage, which is commonly assessed by comparing the volumes of the resulting polytopes. Since directly computing the volume of high-dimensional polytopes is computationally intractable, a sampling-based method is employed, which is explained by

Authorized licensed use limited to: TU Delft Library. Downloaded on September 07,2026 at 09:48:45 UTC from IEEE Xplore. Restrictions apply.

an example as illustrated in Fig. 8. Two polytopes, referred to as polytope A (red) and B (blue), with the true volumes of V_A and V_B are assumed for comparison. An equal number of points are uniformly sampled within each of the two polytopes using the hit-and-run algorithm [23]. Let the number of sampled points that fall within both approximations be α_A and α_B, respectively. The volume ratio V_A/V_B can then be estimated by α_B/α_A. One concern with directly comparing volumes is that as the dimension increases, the growth of volume is exponential, which means that even the smallest difference between polytopes in high-dimensional space results in a huge volume difference. For example, a 24-D cube with an edge length of 1.01 has a volume of 1.27, making it 27% larger than a cube with an edge length of 1. To provide a more intuitive metric, we adopted the geometric mean of the estimated volume ratio (GMVR):

$$GMVR = \left(\frac{\alpha^{\text{ref}}}{\alpha_i}\right)^{\frac{1}{\tau}} \tag{37}$$

Another aspect of performance evaluation is disaggregation feasibility, which measures the degree of overestimation. This is assessed by uniformly sampling points within the approximated polytope and checking their disaggregation feasibility. Since the polytope is an approximation of a Minkowski sum or a projection, two optimization problems are introduced for this purpose:

$$\min_{\boldsymbol{x}_k} 1, \text{ s.t.: } \boldsymbol{A}_k\boldsymbol{x}_k \le \boldsymbol{b}_k, \sum_{k\in\mathcal{K}} \boldsymbol{x}_k = \boldsymbol{x}^{\text{sample}} \tag{38a}$$

$$\min_{\boldsymbol{x}_0} 1, \text{ s.t.: } \begin{bmatrix}\boldsymbol{A} & \boldsymbol{B}\end{bmatrix}\begin{bmatrix}\boldsymbol{x}_0 \\ \boldsymbol{x}^{\text{sample}}\end{bmatrix} \le \boldsymbol{d} \tag{38b}$$

where $\boldsymbol{x}^{\text{sample}}$ represents a sample point. Note that although in our paper the Minkowski sum is formulated as a projection problem, the two are not equivalent. When network constraints are integrated as in (36), the aggregation is still formulated as a projection, but it is no longer a Minkowski sum. Meanwhile, many existing Minkowski sum approximation methods, e.g., the one used for comparison in our case study [10], do not adopt a projection formulation. Thus, for Minkowski sum approximation, (38a) is solved, where $(\boldsymbol{A}_k, \boldsymbol{b}_k)$ represent the individual component polytopes. For projection approximation, (38b) is solved, where $([\boldsymbol{A}, \boldsymbol{B}], \boldsymbol{d})$ defines the original high-dimensional polytope before projection. The number of sampled points that can be successfully disaggregated is used to calculate the geometric average successful disaggregation rate (ASDR), serving as another metric. It works together with GMVR to evaluate an approximation algorithm.

C. A Simple Test Case

In this simple test case, 3 time steps are considered, and a small number of DERs are aggregated, allowing for the exact results to be obtained and visualized.

1) Aggregating DERs With Time Heterogeneity: To verify that the proposed projection-based aggregation formulation can effectively integrate DERs with heterogeneous available times, 2 EV charging events are considered, with parameters shown in Table II.

TABLE II
PARAMETER SETTINGS FOR 2 EV CHARGING EVENTS

	Max. Charging Power (KW)	Initial / Target Energy (kWh)	Charging Efficiency	Available Time (h)
EV1	3	15 / 16.48	0.88	[0,2]
EV2	8.23	12.61 / 20.89	0.91	[1,3]

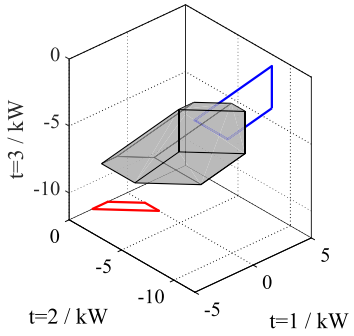


Fig. 9. Aggregation result of 2 EV charging events with heterogeneous available times. The red and blue polytopes correspond to EV1 and EV2, respectively, while the gray polytope represents the aggregated flexibility.

TABLE III
PARAMETER SETTINGS FOR 4 HVACS

	$\overline{P}$ (kW)	$[\underline{T}, \overline{T}, T_0]$ (°C)	$[\eta, \alpha]$	w_t (°C)
HVAC1	110	[22,26,26]	[1.04,-0.05]	[32.4,34.4,34.9]
HVAC2	88	[22,26,26]	[1.04,-0.05]	[32.4,34.4,34.9]
HVAC3	104	[22,26,22]	[1.04,-0.05]	[32.4,34.4,34.9]
HVAC4	93	[22,26,24]	[1.04,-0.05]	[32.4,34.4,34.9]

Fig. 9 illustrates how the established polytope model corresponds to the two EVs after removing state heterogeneity (red and blue) and their aggregation result (gray). As shown in the figure, both EVs are only available during parts of the overall time period, causing their polytopes to degenerate into subspaces. However, for the aggregator, there is always at least one EV available, resulting in an aggregated polytope that extends through the entire dimension.

2) Aggregating Multiple DERs: To verify the performance of the proposed projection-based aggregation formulation and the LP-based projection MIA algorithm, 4 HVACs are aggregated, with parameters summarized in Table III. The vertex enumeration method is used to obtain exact results, while the outer approximation serves as a baseline. The Minkowski formulation approximation method using homothets [10] and the projection formulation approximation method using bound shrinking [16] are included for comparison, both of which are considered state-of-the-art.

As summarized in Table IV and visualized in Fig. 10, both the proposed method and the bound shrinking achieve higher GMVR than the homothets, benefiting from the projection formulation that prevents error accumulation when aggregating multiple DERs. While both the proposed method and the homothets maintain 100% ASDR, the bound shrinking

Authorized licensed use limited to: TU Delft Library. Downloaded on September 07,2026 at 09:48:45 UTC from IEEE Xplore. Restrictions apply.

TABLE IV
RESULTS COMPARISON OF AGGREGATING 4 HVACS IN A SIMPLE TEST CASE

	Exact (Vertex Enumeration)	Algorithm 1 (Proposed)	[16] (Bound Shrinking)	[10] (Homothets)	Outer Approximation
GMVR	-	91.73%	**98.18%**	83.06%	101.57%
ASDR	-	**100.00%**	99.62%	**100.00%**	98.46%
Time / s	5.30	0.30	1.11	0.45	**0.06**

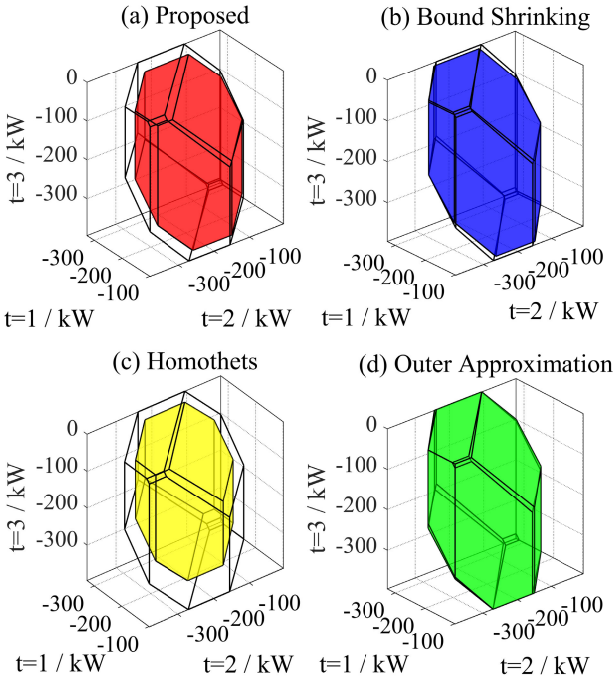


Fig. 10. Results visualization of aggregating 4 HVACs in a simple test case. The colored polytopes represent approximations using different methods, while the transparent polytope shows the exact result.

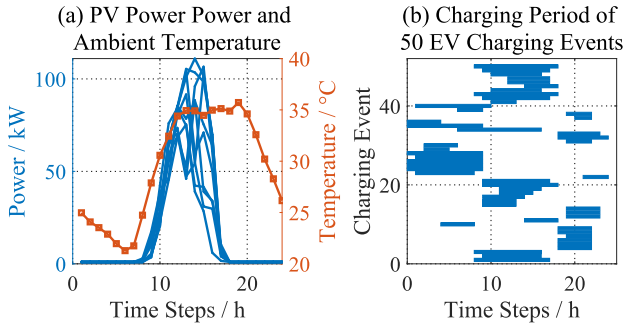


Fig. 11. Parameter settings for PVs, HVACs, and EV charging events in the larger test case.

TABLE V
ACCURACY VALIDATION OF VECTOR ADDITION IN THE MINKOWSKI-CLOSED FAMILY

Dimension	GMVR of the Proposed Method (Vector Addition as Reference)	ASDR of Vector Addition
2	100.00%	100.00%
3	100.00%	100.00%
4	100.00%	100.00%
5	100.00%	99.98%
6	100.00%	100.00%
7	100.00%	99.96%
8	100.00%	99.99%

approach does not strictly serve as an inner approximation, which will be further demonstrated in larger test cases. In [16], the bound shrinking is applied to an outer approximation but only along limited directions, potentially causing disaggregation infeasibility. The proposed method sacrifices 6.45% of flexibility coverage to ensure an inner approximation compared to the bound shrinking, and in turn, improves flexibility coverage by 8.67% compared to the homothets, which is also an inner approximation.

Regarding computation time, due to the small scale of this test case, the exact method remains highly efficient, and none of the approximation methods have a clear advantage.

D. A Larger Test Case

In this case, we evaluate the performance of aggregation algorithms on a 33-bus radial distribution system [24]. The system includes three aggregators located at nodes 5, 19, and 22, responsible for aggregating 10 PVs, 10 HVACs, and 50 EV charging events, respectively. A total of 24 time steps are considered. The PV output profile and ambient temperature for HVACs are shown in Fig. 11(a), while the charging periods of the EVs are shown in Fig. 11(b). Each aggregator performs local aggregation at its corresponding node, followed by a secondary aggregation across the three sites.

1) Validation of Closure Property: We first verify the accuracy of vector addition in the Minkowski-closed family. Two polytopes in minimal H-representation sharing the same LHS matrix are randomly generated in dimensions 2 to 8. The Minkowski sums are computed using vector addition according to Proposition 1. The ASDR is calculated to quantify the degree of overestimation, and the results are used as a reference to evaluate the GMVR of the proposed method. As shown in Table V, except for negligible numerical errors explained in Remark 2, the ASDR equals 100% in all cases, and the GMVR of the proposed method is also 100%, indicating that it provides identical flexibility coverage to vector addition. These results confirm the accuracy of vector addition within the Minkowski-closed family.

2) Aggregation Without Network Constraints: In the primary aggregation, the proposed method, bound shrinking, and

Authorized licensed use limited to: TU Delft Library. Downloaded on September 07,2026 at 09:48:45 UTC from IEEE Xplore. Restrictions apply.

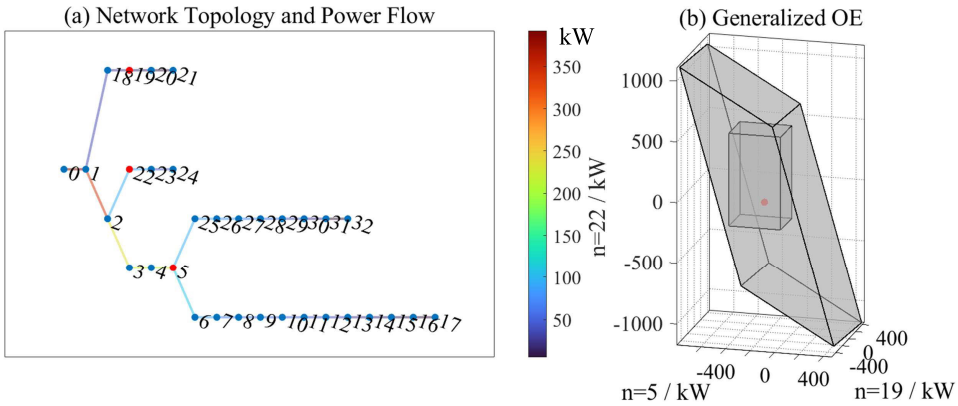


Fig. 12. (a) Topology of the 33-bus radial distribution system, with colors showing the baseline power flow. (b) Visualization of the conventional OE (inside) and generalized OE (outside) corresponding to flexible nodes 5, 19, and 22. The red dot indicates the baseline operating point.

TABLE VI
RESULTS COMPARISON OF AGGREGATION IN A LARGER CASE

	Algorithm 1 (Proposed)	[16] (Bound Shrinking)	Outer Approximation
GMVR	80.20%	87.93%	**100%**
ASDR	**99.97%**	97.68%	84.59%
Time / s	38.88	81.90	**10.06**

outer approximation are adopted, respectively. The homothets method is not applicable in this case, as it cannot accommodate time heterogeneity. In the secondary aggregation, the process is performed without considering network constraints, and vector addition is applied. The results are summarized in Table VI.

As shown in the results, the ASDR of the outer approximation method is 84.59%, indicating higher disaggregation feasibility compared with the smaller case. A similar issue is observed for the bound shrinking method, where the ASDR is only 97.68%. This suggests that when aggregating more diverse DERs in higher-dimensional scenarios, the bound-shrinking strategy becomes less effective in reducing overestimation. In contrast, the proposed method maintains a high ASDR of 99.97%, ensuring a strict inner approximation. Intuitively, to guarantee a strict inner approximation, some flexibility must be sacrificed. In this case, the ASDR increases by 2.29%, while the GMVR decreases by 7.73%.

Regarding computation time, the outer approximation method, without additional steps to improve disaggregation feasibility, is the most efficient. Both the proposed method and the bound shrinking incorporate revisions based on the outer approximation result. As shown, the proposed method, due to its linear nature, is much more efficient than the MILP-based bound shrinking, achieving a 52.53% reduction in computation time. Overall, the proposed method demonstrates the most favorable performance among the three.

3) Integrating Network Constraints: Network constraints are then integrated into the secondary aggregation process. Since the aggregators are located at nodes 5, 19, and 22, a generalized OE can be formulated as a polytope in a 3-D space, as shown in Fig. 12(b), representing the node-coupled

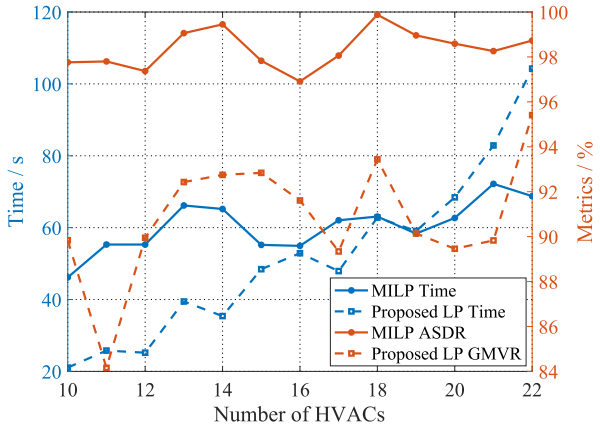


Fig. 13. Computation time and evaluation metrics for aggregating different numbers of HVACs using the proposed method and the bound-shrinking.

capacity range. For comparison, the conventional OE is also calculated. As shown in the figure, the conventional OE, which cannot capture the coupling among nodes, essentially corresponds to a box-shaped MIA of the proposed generalized OE, making it more conservative. In this case, the GMVR of the conventional OE is only 46.84% when the generalized OE is used as the reference. As also depicted in Fig. 12, the power injections at nodes 5 and 22 demonstrate stronger coupling. This can be explained based on the network topology since both nodes are connected to node 2, a heavily loaded bus.

Using the aggregation result without considering network constraints as a reference, the GMVR of the result with network constraints is 88.14%. This indicates that the network constraints reduce the aggregated flexibility range by 11.86%.

E. Sensitivity Analysis

1) Scalability: To evaluate the scalability of the proposed method for larger clusters of DERs, a sensitivity test is performed by aggregating 10 to 22 HVACs. Both the proposed method and the bound shrinking are implemented, and the computation time along with the corresponding ASDR and GMVR are recorded for comparison. The results are shown in Fig. 13.

In terms of computation time, the proposed method clearly outperforms when aggregating up to 18 DERs. For example,

Authorized licensed use limited to: TU Delft Library. Downloaded on September 07,2026 at 09:48:45 UTC from IEEE Xplore. Restrictions apply.

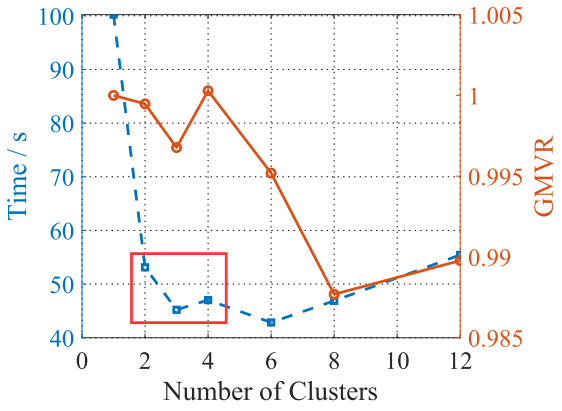


Fig. 14. Computation time and GMVR variation with respect to the number of clusters.

when aggregating 10 HVACs, it takes only 45.62% of the time required by bound shrinking. However, for larger clusters, the computation time of the proposed method grows polynomially, while that of the bound shrinking increases roughly linearly. When the number of HVACs reaches 22, the proposed method takes 51.63% more time than the bound shrinking method. This is because, although the proposed method is LP-based, the number of constraints increases quadratically with the number of DERs, whereas bound shrinking always solves minor MILP problems iteratively. In practice, a clustering strategy can be adopted, and it is recommended to keep the number of DERs in each cluster during primary aggregation below 15 for better computational efficiency.

Fig. 13 also presents the ASDR and GMVR values as the number of HVACs increases. Since the proposed method consistently achieves 100% ASDR and the bound shrinking serves as the reference for calculating GMVR, only the ASDR of the bound shrinking and the GMVR of the proposed method are shown. The results suggest that both indices remain stable and are not significantly impacted by the aggregation scale. The ASDR of the bound shrinking fluctuates around 98%, while the GMVR of the proposed method stays around 90%, consistent with the observations in Table VI.

2) Aggregation by Clusters: The previous case shows that when the proposed method aggregates a large number of DERs simultaneously (e.g., more than 15), the computation time increases significantly. To improve computational efficiency, a hierarchical framework is suggested. However, as the number of clusters grows, even though the computation within each cluster speeds up, the add up time might not decrease. Additionally, approximation errors within each cluster might accumulate, resulting in a decrease in overall accuracy. To evaluate this effect, 24 HVACs are aggregated using the hierarchical framework. They are divided into 1, 2, 3, 4, 6, 8, and 12 clusters, respectively. Primary aggregations within each cluster are performed using the proposed method, followed by secondary aggregation across clusters via vector addition. The number of clusters, along with the corresponding computation time and GMVR, are shown in Fig. 14.

As illustrated, dividing the HVACs into 2, 3, or 4 clusters (marked by the red box in the figure) introduces only minor additional errors while greatly reducing the size of the LPs required to solve the MIA problem. As a result, computation time decreases rapidly while GMVR remains high. However, as the number of clusters grows, accumulated approximation errors cause a sharp decline in GMVR, and solving more LPs slowly increases the total computation time.

VII. Conclusion

This paper presents a novel projection-based DER aggregation model and an LP-based MIA algorithm. Numerical tests verify their effectiveness in handling time heterogeneity and their accuracy and efficiency in large-scale aggregation. In a case study involving 10 PVs, 10 HVACs, and 50 EV charging events over 24 time steps, the proposed method achieves a strict inner approximation with accuracy comparable to the existing bound shrinking method, while improving computational efficiency by 52.53%. Sensitivity analysis further demonstrates that the proposed method maintains a clear computational advantage when aggregating up to 15 HVACs. For larger-scale scenarios, a hierarchical framework is introduced, within which a Minkowski-closed family is proven and verified, enabling accurate and efficient secondary aggregation via vector addition. The sensitivity analysis also shows that dividing 24 HVACs into 2–4 clusters yields substantial computational savings with negligible accuracy loss. In addition, generalized OEs are formulated based on the LinDistFlow model and incorporated into the aggregation framework, allowing DSOs to communicate network constraints to aggregators without revealing sensitive information. Tests on the 33-bus distribution system indicate that the generalized OEs expand the feasible region coverage by 53.15% compared with conventional OEs.

Despite these advantages, the hierarchical framework remains necessary for large-scale aggregation, as the number of LP constraints grows quadratically with the number of DERs, affecting efficiency. Moreover, the LinDistFlow-based construction of security constraints depends on convex relaxation and linearization, which ignore network losses. Developing more scalable algorithms and more accurate integration of network constraints represents a promising direction for future work.

References

[1] H. Liang, Y. Liu, F. Li, and Y. Shen, "Dynamic economic/emission dispatch including PEVs for peak shaving and valley filling," *IEEE Trans. Ind. Electron.*, vol. 66, no. 4, pp. 2880–2890, Apr. 2019.

[2] D. Koraki and K. Strunz, "Wind and solar power integration in electricity markets and distribution networks through service-centric virtual power plants," *IEEE Trans. Power Syst.*, vol. 33, no. 1, pp. 473–485, Jan. 2018.

[3] S. Barot and J. A. Taylor, "A concise, approximate representation of a collection of loads described by polytopes," *Int. J. Electr. Power Energy Syst.*, vol. 84, pp. 55–63, Jan. 2017.

[4] F. L. Müller, J. Szabó, O. Sundström, and J. Lygeros, "Aggregation and disaggregation of energetic flexibility from distributed energy resources," *IEEE Trans. Smart Grid*, vol. 10, no. 2, pp. 1205–1214, Mar. 2019.

[5] Z. Yi, Y. Xu, W. Gu, L. Yang, and H. Sun, "Aggregate operation model for numerous small-capacity distributed energy resources considering uncertainty," *IEEE Trans. Smart Grid*, vol. 12, no. 5, pp. 4208–4224, Sep. 2021.

[6] M. S. Nazir, I. A. Hiskens, A. Bernstein, and E. Dall'Anese, "Inner approximation of Minkowski sums: A union-based approach and applications to aggregated energy resources," in *Proc. IEEE Conf. Decis. Control (CDC)*, Dec. 2018, pp. 5708–5715.

Authorized licensed use limited to: TU Delft Library. Downloaded on September 07,2026 at 09:48:45 UTC from IEEE Xplore. Restrictions apply.

[7] X. Chen, E. Dall'Anese, C. Zhao, and N. Li, "Aggregate power flexibility in unbalanced distribution systems," *IEEE Trans. Smart Grid*, vol. 11, no. 1, pp. 258–269, Jan. 2020.
[8] E. Polymeneas and S. Meliopoulos, "Aggregate modeling of distribution systems for multi-period OPF," in *Proc. Power Syst. Comput. Conf. (PSCC)*, Jun. 2016, pp. 1–8.
[9] L. Zhao, W. Zhang, H. Hao, and K. Kalsi, "A geometric approach to aggregate flexibility modeling of thermostatically controlled loads," *IEEE Trans. Power Syst.*, vol. 32, no. 6, pp. 4721–4731, Nov. 2017.
[10] M. Zhang, Y. Xu, X. Shi, and Q. Guo, "A fast polytope-based approach for aggregating large-scale electric vehicles in the joint market under uncertainty," *IEEE Trans. Smart Grid*, vol. 15, no. 1, pp. 701–713, Jan. 2024.
[11] C. Li, K. Zheng, C. Feng, Q. Chen, and P. P. Vergara, "Modeling and aggregating DER flexibility region in VPPs: An elimination and projection approach," in *Proc. IEEE Power Energy Soc. Gen. Meeting (PESGM)*, Jul. 2024, pp. 1–5.
[12] H. Moring, S. Jang, N. Ozay, and J. L. Mathieu, "Nodal operating envelopes vs. network-wide constraints: What is better for network-safe coordination of DERs?" *Electric Power Syst. Res.*, vol. 234, Sep. 2024, Art. no. 110702.
[13] B. Liu and J. H. Braslavsky, "Robust dynamic operating envelopes for DER integration in unbalanced distribution networks," *IEEE Trans. Power Syst.*, vol. 39, no. 2, pp. 3921–3936, Mar. 2024.
[14] B. Cui, A. Zamzam, and A. Bernstein, "Network-cognizant time-coupled aggregate flexibility of distribution systems under uncertainties," in *Proc. Amer. Control Conf. (ACC)*, May 2021, pp. 4178–4183.
[15] S. Wang and W. Wu, "Aggregate flexibility of virtual power plants with temporal coupling constraints," *IEEE Trans. Smart Grid*, vol. 12, no. 6, pp. 5043–5051, Nov. 2021.
[16] Y. Wen, Z. Hu, J. He, and Y. Guo, "Improved inner approximation for aggregating power flexibility in active distribution networks and its applications," *IEEE Trans. Smart Grid*, vol. 15, no. 4, pp. 3653–3665, Jul. 2024.
[17] K. Fukuda and A. Prodon, "Double description method revisited," in *Proc. Franco-Jpn. Franco-Chin. Conf. Combinatorics Comput. Sci.*Berlin, Germany: Springer, 1995, pp. 91–111.
[18] G. B. Dantzig and B. C. Eaves, "Fourier–Motzkin elimination and its dual," *J. Combinat. Theory, A*, vol. 14, no. 3, pp. 288–297, 1973, doi: 10.1016/0097-3165(73)90004-6. [Online]. Available: https://www.sciencedirect.com/science/article/pii/0097316573900046
[19] Y. Wen, Z. Hu, and L. Liu, "Aggregate temporally coupled power flexibility of DERs considering distribution system security constraints," *IEEE Trans. Power Syst.*, vol. 38, no. 4, pp. 3884–3896, Jul. 2023.
[20] R.-J. Jing, M. Moreno-Maza, and D. Talaashrafi, "Complexity estimates for Fourier-motzkin elimination," in *Proc. 22nd Int. Workshop Comput. Algebra Sci. Comput.*, Linz, Austria. Cham, Switzerland: Springer, 2020, pp. 282–306.
[21] G. M. Ziegler, *Lectures on Polytopes*, vol. 152. Cham, Switzerland: Springer, 2012.
[22] M. Baran and F. F. Wu, "Optimal sizing of capacitors placed on a radial distribution system," *IEEE Trans. Power Del.*, vol. 4, no. 1, pp. 735–743, Jan. 1989.
[23] D. E. Kaufman and R. L. Smith, "Direction choice for accelerated convergence in hit-and-run sampling," *Oper. Res.*, vol. 46, no. 1, pp. 84–95, Feb. 1998.
[24] M. E. Baran and F. F. Wu, "Network reconfiguration in distribution systems for loss reduction and load balancing," *IEEE Trans. Power Del.*, vol. 4, no. 2, pp. 1401–1407, Apr. 1989.



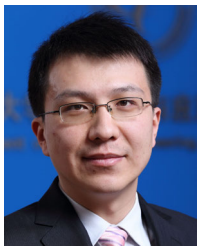
Chuyi Li (Graduate Student Member, IEEE) received the B.S. degree in electrical engineering from the Huazhong University of Science and Technology, Wuhan, China, in 2021. He is currently pursuing the Ph.D. degree in electrical engineering with Tsinghua University, Beijing, China. During his doctoral studies, from October 2023 to 2024, he was a Guest Researcher with the Intelligent Electrical Power Grids (IEPG) Group, Delft University of Technology, Delft, The Netherlands. His research interests include distributed energy resource aggregation, computation-power optimization for data centers, and non-intrusive load monitoring.



Kedi Zheng (Member, IEEE) received the B.S. and Ph.D. degrees in electrical engineering from Tsinghua University, Beijing, China, in 2017 and 2022, respectively. He is currently a Post-Doctoral Researcher with Tsinghua University. He is also a Visiting Research Associate with The University of Hong Kong. His research interests include data analytics in power systems, electricity markets, and application of big data analytics for electricity market.



Pedro P. Vergara (Senior Member, IEEE) was born in Barranquilla, Colombia, in 1990. He received the B.Sc. degree (Hons.) in electronic engineering from the Universidad Industrial de Santander, Bucaramanga, Colombia, in 2012, the M.Sc. degree in electrical engineering from the State University of Campinas (UNICAMP), Campinas, Brazil, in 2015, and the joint Ph.D. degree from UNICAMP, and the University of Southern Denmark (SDU), Denmark, in 2019, funded by São Paulo Research Foundation (FAPESP). In 2019, he joined Eindhoven University of Technology (TU/e), The Netherlands, as a Post-Doctoral Researcher. In 2020, he was appointed as an Assistant Professor with the Intelligent Electrical Power Grids (IEPG) Group, Delft University of Technology, The Netherlands. He is currently an Associate Professor with Delft University of Technology. His main research interests include the development of algorithms for the control, planning, and operation of electrical distribution systems with high penetration of low-carbon energy resources (e.g, electrical vehicles, PV systems, and electric heat pumps) using optimization and machine learning approaches. He received the Best Presentation Award at the Summer Optimization School in 2018 organized by the Technical University of Denmark (DTU) and the Best Paper Award at the 3rd IEEE International Conference on Smart Energy Systems and Technologies (SEST), Türkiye, in 2020.



Ning Zhang (Senior Member, IEEE) received the B.S. and Ph.D. degrees from the Electrical Engineering Department, Tsinghua University, China, in 2007 and 2012, respectively. He is currently an Associate Professor with Tsinghua University. His research interests include renewable energy, and power system planning and operation, and multiple energy systems integration.



Hongye Guo (Member, IEEE) received the B.S. and Ph.D. degrees in electrical engineering from Tsinghua University in 2015 and 2020 respectively. In 2020, he was a Post-Doctoral Researcher with Tsinghua University. He has been with Tsinghua University, since he completed his Postdoctoral Research in 2022. He is currently an Associate Professor with the Department of Electrical Engineering and the Director of the Energy Trading Platform Research Office with the Institute of Energy Internet Research Institute, Tsinghua University. His research interests include electricity markets, demand side flexibility, and applications of artificial intelligence in power systems.

Authorized licensed use limited to: TU Delft Library. Downloaded on September 07,2026 at 09:48:45 UTC from IEEE Xplore. Restrictions apply.